MRI Brain-print as secure hidden bio-metric system

A Project Report

submitted by

SURYA RAGHAV B (CS21B2042)

in partial fulfilment of requirements

for the completion of the course

Introduction to Biometrics

Department of Computer Science and Engineering
INDIAN INSTITUTE OF INFORMATION TECHNOLOGY, DESIGN AND MANUFACTURING KANCHEEPURAM

MAY 2024

DECLARATION OF ORIGINALITY

I, **Surya Raghav B**, with Roll No: **CS21B2042** hereby declare that the material presented in the Project Report titled **MRI Brain-print as secure hidden bio-metric system** represents original work carried out by me in the **Department of Computer Science and Engineering** at the Indian Institute of Information Technology, Design and Manufacturing, Kancheepuram.

With my signature, I certify that:

- I have not manipulated any of the data or results.
- I have not committed any plagiarism of intellectual property. I have clearly indicated and referenced the contributions of others.
- I have explicitly acknowledged all collaborative research and discussions.
- I have understood that any false claim will result in severe disciplinary action.
- I have understood that the work may be screened for any form of academic misconduct.

Surya Raghav B

Place: Chennai

Date: 13.05.2024

ACKNOWLEDGEMENTS

I extend my deepest gratitude to all those who have contributed to the successful completion of this project, "MRI Brain-print as secure hidden bio-metric system." My journey through this endeavor has been enriched by the support, guidance, and expertise of numerous individuals and organizations, without whom this project would not have been possible.

First and foremost, I express my sincere appreciation to Dr. Rahul Raman for his invaluable insights throughout the duration of this research by teaching the crucial concepts that directly applied to the project. Their commitment to excellence has been instrumental in shaping the direction and focus of our investigation.

I extend my gratitude to the medical professionals and technicians involved in conducting the MRI scans, whose expertise and precision have ensured the quality and accuracy of the imaging data acquired for our research. Thanks to Open Access Series of Imaging Studies (OASIS) for their clean maintenance of the dataset which has been very crucial for the project.

I am also grateful to the experts and scholars in the field of biometrics and neuroimaging who have generously shared their insights, feedback, and expertise through their outstanding research work enriching our understanding and shaping the development of our methodologies

ABSTRACT

With the continuous evolution of neuroimaging in the medical field, emerging biometric modalities have garnered interest as promising candidates for person recognition. These modalities, categorized under "Hidden Biometrics," leverage clinical measurements and medical imaging for recognition purposes. The utilization of hidden biometrics is motivated by the inherent difficulty in attacking such systems, thereby enhancing robustness in person verification and identification. In this project we present a novel non-invasive approach for person recognition by extracting a unique brain signature termed "brainprint." Specifically, we investigate the cortical regions of volumetric brain MRI (Magnetic Resonance Imaging) images obtained from 21 healthy subjects. Each subject's four 3D cortical surfaces are transformed into 2D cortical folds maps. Brainprints are then constructed from these textures by extracting features using Wavelet Gabor Transform, representing a discriminative signature of the brain. In identification scenarios, this approach achieves a recognition rate of 96.30%.

TABLE OF CONTENTS

ACKNOWLEDGEMENTS **i**

ABSTRACT **ii**

1 Introduction **2**

1.1 Why to use Brain-prints as a hidden bio-metric ? 2

1.2 Biology behind MRI Brain images 3

2 General Methodology **5**

2.1 Processing Phases 5

2.2 Brain Image Acquisition 6

2.3 Image Denoising and Restoration 7

2.3.1 Gaussian filtering 7

2.3.2 Histogram equalization 8

2.3.3 Contraharmonic mean filtering 9

2.4 Feature Extraction 10

2.5 Dimensionality Reduction 11

3 Model Training and Evaluation **13**

3.1 CNN Architecture 13

3.1.1 Explanation of Model Compilation: 14

3.1.2 Explanation of Model Training: 14

3.2 Model Evaluation 15

4 CONCLUSION AND FUTURE SCOPE **17**

4.1 Conclusion 17

4.2 Future Scope 17

CHAPTER 1

Introduction

1.1 Why to use Brain-prints as a hidden bio-metric ?

Nowadays, person identification and verification find increasing utility across various fields and applications, tailored to meet specific security requirements. Among the widely employed biometric modalities, fingerprints, palmprints, iris recognition, and face recognition stand out prominently. These modalities have been extensively integrated into numerous systems and devices, rendering them useful yet vulnerable to potential attacks. Consequently, the biometric community actively endeavors to devise robust solutions to counter identity spoofing threats. Common concerns include fake fingerprints, which have spurred dedicated research efforts. Other modalities susceptible to attacks include iris recognition, 2D/3D facial recognition, and palm-print biometrics, including vein patterns using near-infrared imaging. Despite the emergence of promising solutions to address these challenges, exploring alternative biometric approaches remains compelling.

Recently, a burgeoning category of biometrics, termed hidden biometrics, has garnered attention. Hidden biometrics involve the extraction of features from parts of the human body that are not directly accessible or visible to the naked eye. This approach may necessitate specific devices or equipment commonly found in clinical and medical settings. Examples of hidden biometrics include bio-signals such as EEG (Electroencephalogram), ECG (Electrocardiogram), X-ray imaging, and MRI, among others.

In this study, we focus on exploring human brain images obtained from MRI scans. Our objective is to extract a distinctive brainprint from each 3D brain volumetric image for use in verification or identification tasks. These images contain detailed information about brain folds, encompassing a range of cortical and subcortical structures. Unlike some common biometric modalities, our proposed approach offers a significant advantage: the inherent difficulty in attempting attacks or spoofing. This difficulty arises from

the fact that individuals cannot modify the features of their own brains, thus enhancing the security and robustness of the system.

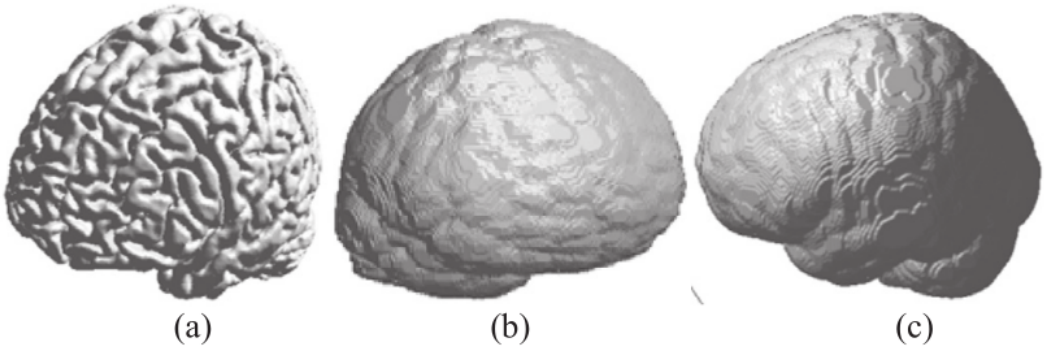

Figure 1.1: View of pial surfaces (a) and inner skull surfaces (b and c)

1.2 Biology behind MRI Brain images

Based on numerous studies, several intriguing questions arise:

- **Are cortical folding patterns unique to each individual?** Evidence suggests that cortical folding patterns, also known as sulco-gyral patterns, are indeed unique to each individual. These patterns form a distinct brainprint that can be used for identification purposes.
- **Are brains truly asymmetric?** While both hemispheres of the brain are similar in size, shape, and weight, they exhibit asymmetry in terms of the distribution of brain tissues (white and gray matter) and the configuration of cortical folds. This asymmetry renders each individual's brain distinct, even in cases of identical twins.
- **Is the shape of individual brain structures heritable?** Recent studies in genetics and neuroscience indicate that genetic factors, including "jumping genes," contribute to the development of brain folds and overall brain morphology. However, environmental factors and experiences also play a role in shaping these structures.
- **Are cortical folds and brain shape stable?** While the gray matter of the brain may undergo changes related to aging and cerebral diseases, studies suggest that the sulco-gyral patterns remain stable and consistent throughout adulthood. This stability reinforces the potential utility of brain folds as biometric traits for verification and identification.

The findings suggest that brain folds and sulco-gyral patterns are highly specific to each individual, making them promising candidates for biometric identification. De-

spite variations in brain morphology related to factors such as aging and disease, the stability of cortical folds underscores their potential as reliable biometric markers. Thus, the question arises: can brain folds be effectively utilized as biometric traits for verification and identification purposes? This question prompts further exploration within the scope of our work.

CHAPTER 2

General Methodology

2.1 Processing Phases

Our approach involves the following processing phases. Here's a brief overview of each phase:

1. **Brain Image Acquisition:** High-resolution structural brain MRI images are utilized due to their non-invasive nature and lack of requirement for radiative contrast medium. These images are provided by the OASIS dataset.
2. **Image Denoising and Restoration:** Prior to feature extraction, it's essential to address any noise or artifacts present in the MRI images. Image denoising techniques, such as Gaussian smoothing, median filtering or contrast stretching can be employed to enhance image quality and remove unwanted noise.
3. **Features Extraction:** Textural features are extracted from the projected curvilinear slices using Gabor transform. This step characterizes the unique patterns present in the cortical folds.
4. **Dimensionality Reduction:** Principal Component Analysis (PCA) is employed to retain only the most relevant characteristics of the brainprints, reducing the complexity of the data while preserving discriminative information.
5. **Performance Evaluation:** Various classifiers are applied to evaluate the performance of the proposed approach. This phase aims to reinforce the hypothesis of the uniqueness of the biometric modality and its suitability for person identification and verification tasks.

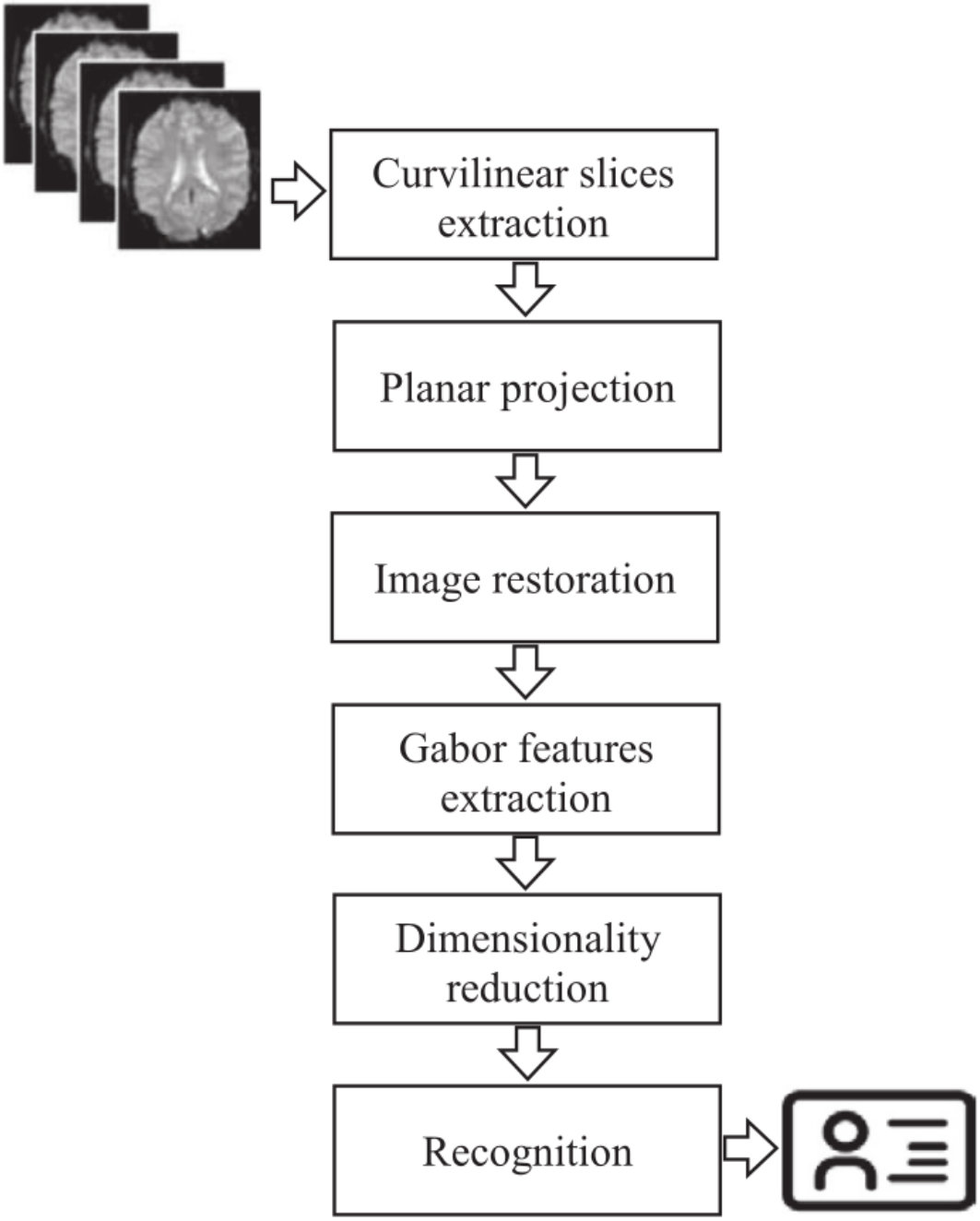

Figure 2.1: Flow chart of the processing

2.2 Brain Image Acquisition

The experimental evaluation of our novel biometric approach, centered on human brain-print recognition, was conducted using the OASIS dataset (Open Access Series of Imaging Studies). This dataset provides volumetric brain MR images, making it an ideal choice due to its availability of images for healthy adult individuals, along with multiple

acquisitions per individual. The OASIS dataset comprises cross-sectional T1-weighted structural MP-RAGE images, each with specific parameters including TR, TE, slice thickness, slice number, flip angle, and in-plane resolution.

In our study, the dataset primarily consisted of MR images corresponding to adult individuals aged between 18 and 55 years, encompassing both sexes, and showing no signs of brain pathology. The dataset was characterized by 220 unique individuals or classes, with each individual having four volumetric MR images available for analysis.

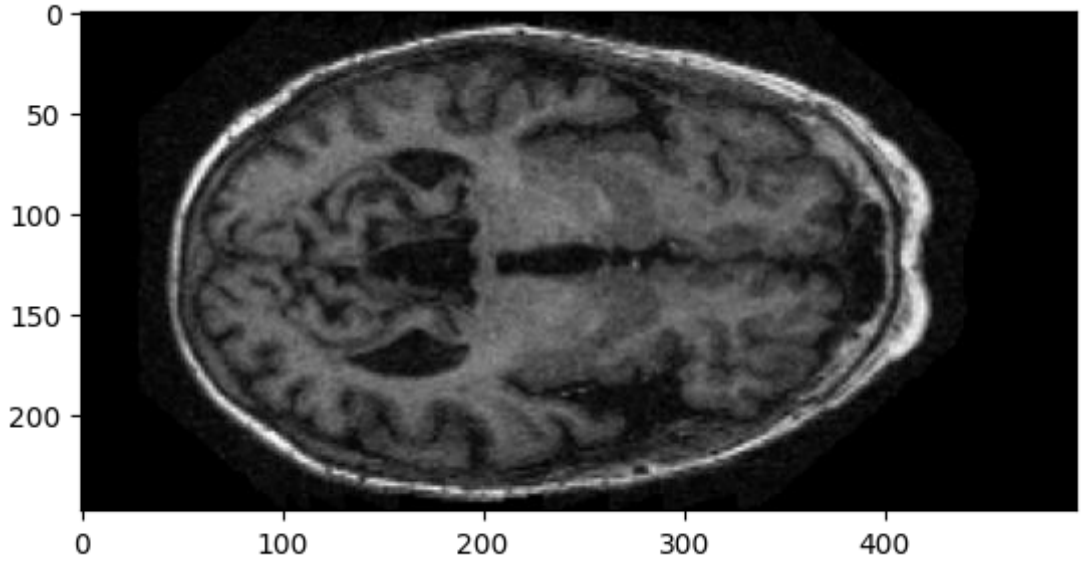

Figure 2.2: Original MR Image

2.3 Image Denoising and Restoration

2.3.1 Gaussian filtering

First we blur the image using a Gaussian filter. This removes any noise artifacts from the image. We sample a discrete Gaussian kernel from the continuous 2D Gaussian distribution given below.

$$f(x, y|\mu_x, \mu_y, \sigma) = \frac{1}{2\pi\sigma^2} \cdot \exp\left(-\frac{(x-\mu_x)^2 + (y-\mu_y)^2}{2\sigma^2}\right)$$

2.3.2 Histogram equalization

Consider a discrete grayscale image $\{x\}$ and let n_i be the number of occurrences of gray level i. The probability of an occurrence of a pixel of level i in the image is

$$p_x(i) = p(x = i) = \frac{n_i}{n}, \quad 0 \leq i < L$$

L being the total number of gray levels in the image (typically 256), n being the total number of pixels in the image, and $p_x(i)$ being in fact the image's histogram for pixel value i, normalized to $[0, 1]$. Let us also define the cumulative distribution function corresponding to i as

$$\mathrm{cdf}_x(i) = \sum_{j=0}^{i} p_x(x = j)$$

which is also the image's accumulated normalized histogram. We would like to create a transformation of the form $y = T(x)$ to produce a new image $\{y\}$, with a flat histogram. Such an image would have a linearized cumulative distribution function (CDF) across the value range, i.e.,

$$\mathrm{cdf}_y(i) = (i + 1)K \quad \text{for} \quad 0 \leq i < L$$

for some constant K. The properties of the CDF allow us to perform such a transform

$$y = T(k) = \mathrm{cdf}_x(k)$$

where k is in the range $[0, L - 1]$. Notice that T maps the levels into the range $[0, 1]$, since we used a normalized histogram of $\{x\}$. In order to map the values back into their original range, the following simple transformation needs to be applied on the result:

$$y' = y \cdot (\max\{x\} - \min\{x\}) + \min\{x\} = y \cdot (L - 1)$$

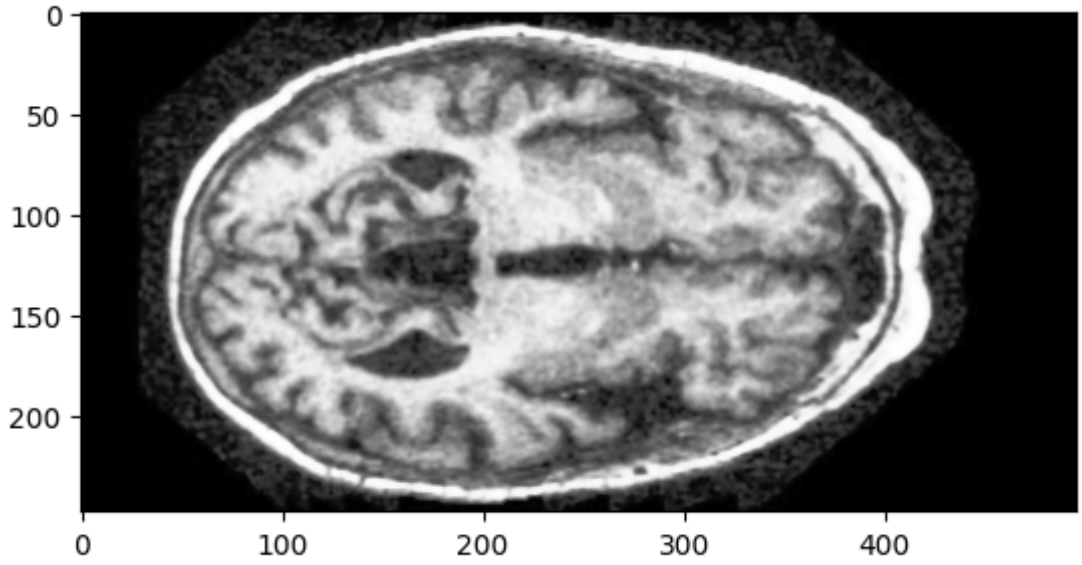

Figure 2.3: Image after Gaussian filtering and Histogram equalization

2.3.3 Contraharmonic mean filtering

Contraharmonic mean filtering is a type of image filtering technique used for image denoising. It is particularly effective in removing salt-and-pepper noise from images while preserving edges. The filter computes the mean of the pixel values raised to a power, which can be adjusted to control the filtering behavior.

Given an image I with pixel values $I(x, y)$, the contraharmonic mean filter of order Q at pixel (x, y) is defined as:

$$I_{\text{contraharmonic}}(x, y) = \frac{\sum_{(s,t)\in S} I(s, t)^{Q+1}}{\sum_{(s,t)\in S} I(s, t)^{Q}}$$

where S is the neighborhood of pixel (x, y) over which the filter is applied. The parameter Q determines the order of the filter, with positive values enhancing the filtering effect for salt noise (positive outliers) and negative values enhancing the filtering effect for pepper noise (negative outliers).

The contraharmonic mean filtering process involves sliding a window over the image, computing the contraharmonic mean within the window at each pixel location, and replacing the original pixel value with the computed mean value. This process effectively removes salt-and-pepper noise while preserving image details and edges.

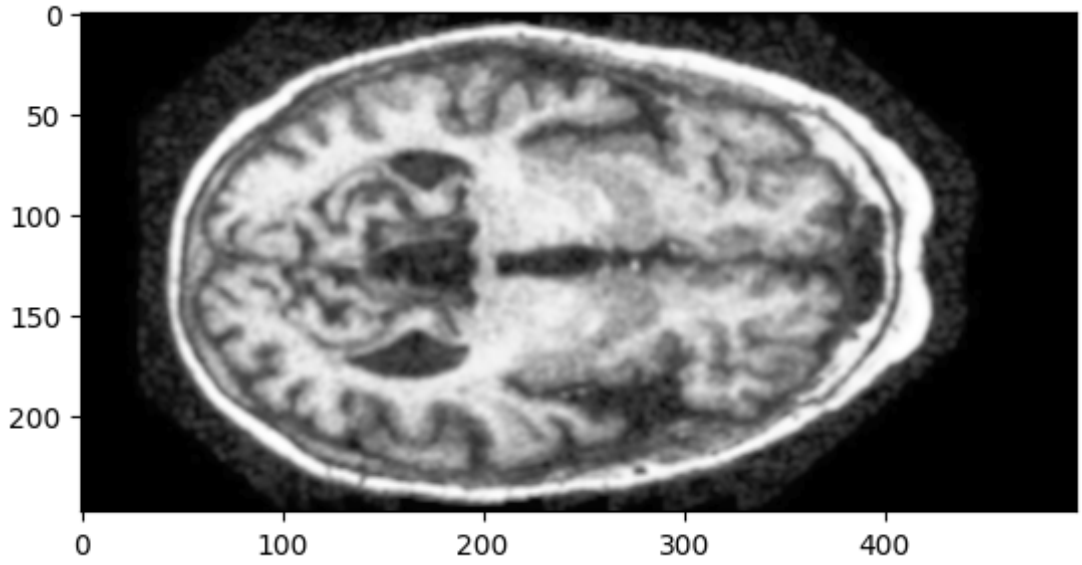

Figure 2.4: Image after Contraharmonic mean filtering

2.4 Feature Extraction

The 2D Gabor wavelet transform is an extension of the 1D Gabor filter to analyze two-dimensional signals such as images. It is widely used in image processing for tasks such as texture analysis, edge detection, and feature extraction.

A 2D Gabor filter is defined as a complex sinusoidal wave modulated by a Gaussian envelope in both the spatial dimensions. Mathematically, the 2D Gabor filter is given by:

$$g(x, y; f, \theta, \sigma_x, \sigma_y, \gamma) = \exp\left(-\frac{x^2}{2\sigma_x^2} - \frac{y^2}{2\sigma_y^2}\right)\cos(2\pi f(x\cos\theta + y\sin\theta))$$

where: x and y are the spatial variables, f is the frequency of the sinusoidal component, θ is the orientation of the filter, σ_x and σ_y are the standard deviations of the Gaussian envelope in the horizontal and vertical directions respectively, γ is the aspect ratio of the elliptical Gaussian envelope.

The 2D Gabor wavelet transform is obtained by convolving the input image with a bank of Gabor filters at different scales, orientations, and aspect ratios. This results in a multi-scale, multi-orientation representation of the image, capturing both the frequency

and spatial information at different levels.

The transformed image, known as the Gabor response, encodes local texture features, edges, and other image structures. It is commonly used as a feature descriptor in various computer vision tasks such as object recognition, texture classification, and image segmentation.

The Gabor wavelet transform offers advantages such as orientation selectivity, spatial localization, and frequency selectivity, making it a powerful tool for analyzing complex image patterns.

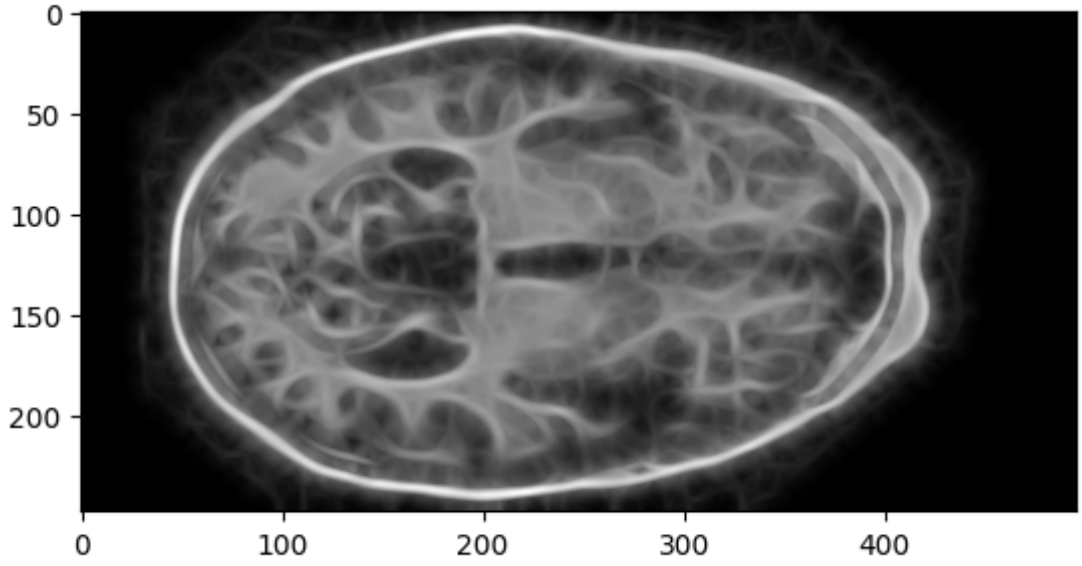

Figure 2.5: Image after Gabor wavelet filtering

2.5 Dimensionality Reduction

Principal Component Analysis (PCA) is a dimensionality reduction technique used to extract important information from high-dimensional data by projecting it onto a lower-dimensional subspace. It identifies the directions (principal components) that capture the maximum variance in the data. Let $\mathbf{X}$ be the data matrix with n observations and m variables. The first step in PCA is to center the data by subtracting the mean of each variable:

$$\mathbf{X}_{\text{centered}} = \mathbf{X} - \bar{\mathbf{x}}$$

where $\bar{\mathbf{x}}$ is the mean vector. Next, PCA computes the covariance matrix $\mathbf{C}$ of the centered data:

$$\mathbf{C} = \frac{1}{n-1}\mathbf{X}_{\text{centered}}^{T}\mathbf{X}_{\text{centered}}$$

The eigenvectors $\mathbf{v}_1, \mathbf{v}_2, ..., \mathbf{v}_m$ of the covariance matrix correspond to the principal components, and the corresponding eigenvalues $\lambda_1, \lambda_2, ..., \lambda_m$ represent the amount of variance explained by each principal component. PCA selects the top k eigenvectors (principal components) corresponding to the largest k eigenvalues to form the projection matrix $\mathbf{W}$:

$$\mathbf{W} = [\mathbf{v}_1, \mathbf{v}_2, ..., \mathbf{v}_k]$$

Finally, PCA projects the centered data onto the lower-dimensional subspace spanned by the selected principal components:

$$\mathbf{Y} = \mathbf{X}_{\text{centered}}\mathbf{W}$$

where $\mathbf{Y}$ is the projected data matrix. After PCA our feature vector dimension would be reduced but still captures the important information.

CHAPTER 3

Model Training and Evaluation

3.1 CNN Architecture

Layer (type)	Output Shape	Param #
Conv2D	(None, 248, 64, 32)	160
Conv2D	(None, 248, 64, 32)	4,128
BatchNormalization	(None, 248, 64, 32)	128
MaxPooling2D	(None, 124, 32, 32)	0
Dropout	(None, 124, 32, 32)	0
Conv2D	(None, 124, 32, 64)	8,256
Conv2D	(None, 124, 32, 64)	16,448
BatchNormalization	(None, 124, 32, 64)	256
MaxPooling2D	(None, 62, 16, 64)	0
Dropout	(None, 62, 16, 64)	0
Flatten	(None, 63488)	0
Dense	(None, 512)	32,506,368
Dropout	(None, 512)	0
Dense	(None, 21)	10,773

Table 3.1: Model Architecture

Total params: 32,546,517 (124.16 MB)

Trainable params: 32,546,325 (124.15 MB)

Non-trainable params: 192 (768.00 B)

1. **Conv2D**: This layer represents a 2D convolutional layer. It applies convolution operation to the input, resulting in feature maps. The output shape is (None, 248, 64, 32), meaning it has 32 filters of size 64x64, with a stride of 1 and 'valid' padding.

2. **Conv2D_1**: Another 2D convolutional layer with the same output shape as the previous layer but with different parameters.

3. **BatchNormalization**: This layer normalizes the activations of the previous layer at each batch. It helps in speeding up the training process and reducing the risk of overfitting.

4. **MaxPooling2D**: This layer performs max pooling operation for spatial data reduction. It reduces the dimensionality of each feature map but retains the most important information.
5. **Dropout**: This layer applies dropout regularization, randomly setting a fraction of input units to 0 at each update during training. It helps prevent overfitting.
6. **Flatten**: This layer flattens the input, converting it into a 1D array. It prepares the data for input into the fully connected layers.
7. **Dense**: Fully connected layer with 512 units, followed by a ReLU activation function.
8. **Dense_1**: Fully connected layer with 21 units, representing the output classes of the model.

3.1.1 Explanation of Model Compilation:

```
model.compile(loss='categorical_crossentropy', optimizer='Adamax',
    metrics=['accuracy'])
```

The first line of code compiles the model. It sets up the model for training by specifying the loss function, optimizer, and evaluation metrics. Here's the breakdown:

- `loss='categorical_crossentropy'`: This specifies the loss function used during training. Categorical cross-entropy is commonly used for multi-class classification problems.
- `optimizer='Adamax'`: This specifies the optimizer used to update the weights of the network during training. Adamax is a variant of the Adam optimizer, which is an adaptive learning rate optimization algorithm.
- `metrics=['accuracy']`: This specifies the evaluation metric used to monitor the performance of the model during training. In this case, it's accuracy, which measures the proportion of correctly classified samples.

3.1.2 Explanation of Model Training:

```
model.fit(x_train, y_train, epochs=10, batch_size=10, verbose=1,
    validation_data=(x_test, y_test))
```

The second line of code trains the model using the compiled settings. Here's the breakdown:

- This line of code fits the model to the training data (`x_train` and `y_train`).

- `epochs=10`: This specifies the number of epochs, i.e., the number of times the entire training dataset is passed forward and backward through the neural network.
- `batch_size=10`: This specifies the number of samples per gradient update. In this case, 10 samples will be processed before updating the weights of the model.
- `verbose=1`: This parameter controls the verbosity of the training process. A value of 1 indicates that progress bars will be displayed during training.
- `validation_data=(x_test,y_test)`: This specifies the validation data to be used during training. The model will be evaluated on this data after each epoch to monitor its performance and detect overfitting.

3.2 Model Evaluation

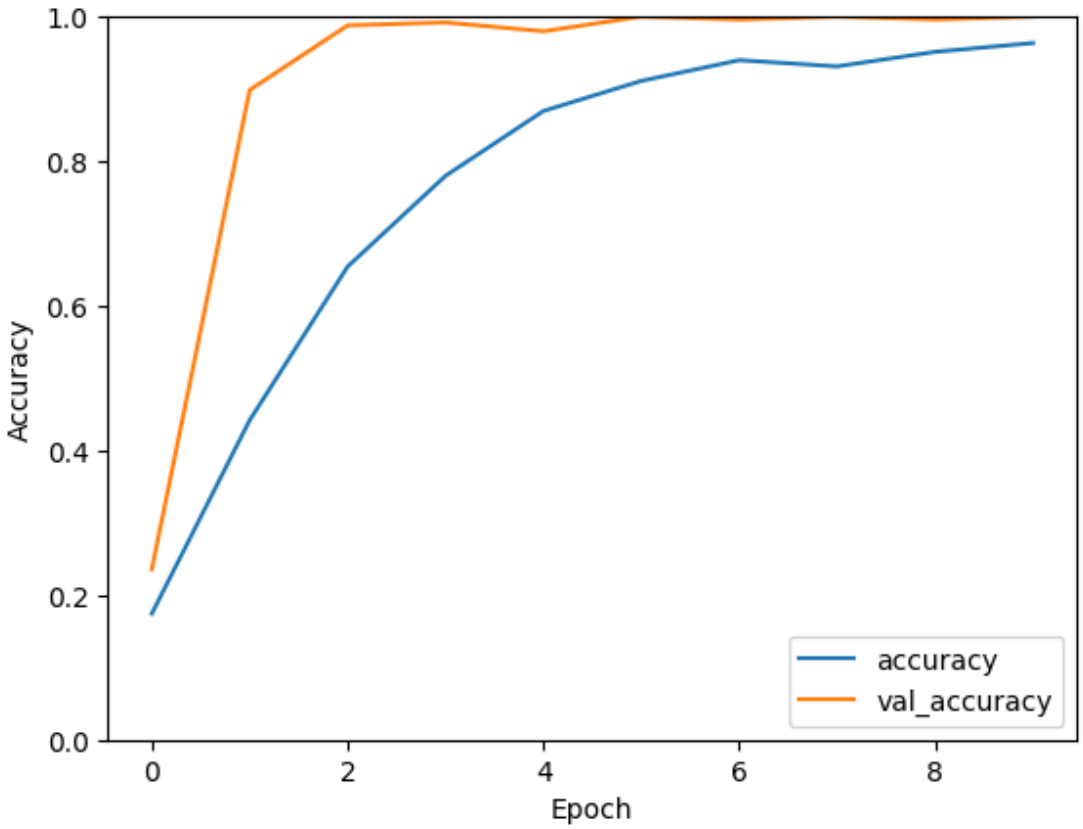

Figure 3.1: Accuracy vs Epochs plot

The plot displays the training accuracy and validation accuracy curves of a model over training epochs. The accuracy curve increases smoothly, while the validation accuracy curve rises steeply initially before leveling off, as expected during model training. Our

model finally settles at an accuracy of 96.30%, with the validation accuracy almost reaching 100%

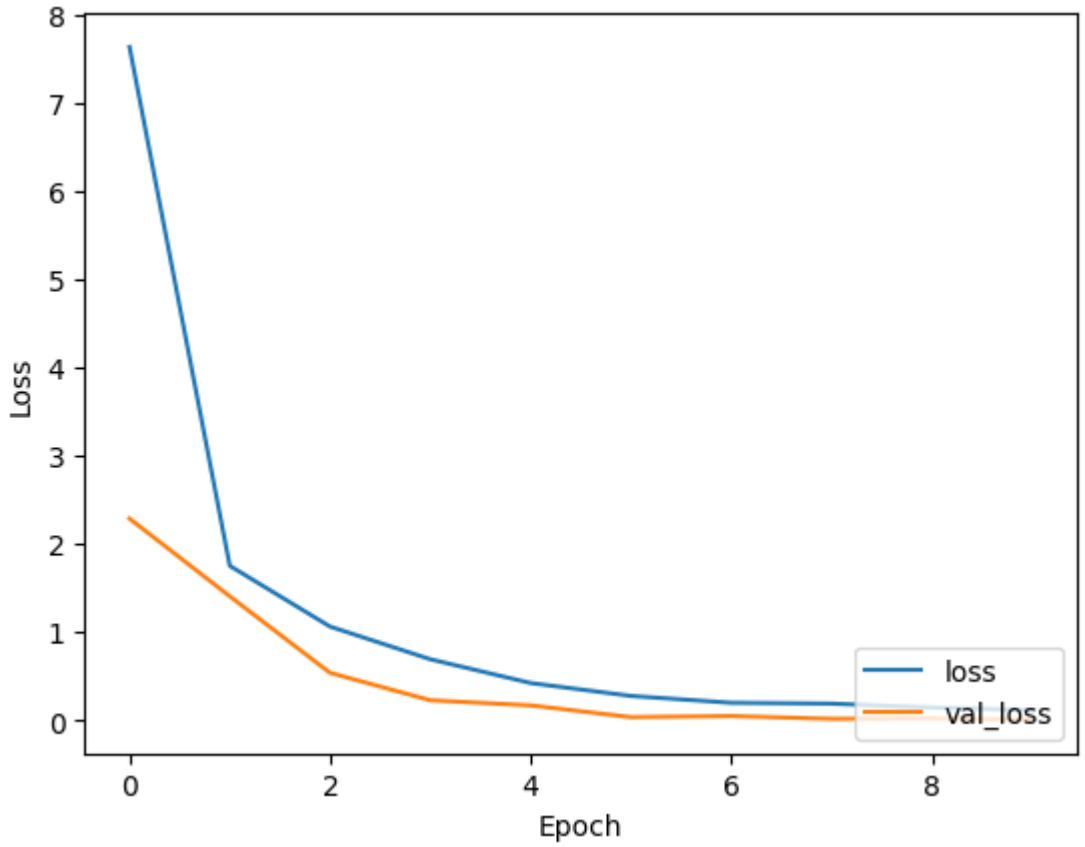

Figure 3.2: Loss vs Epochs plot

The plot displays the training loss and validation loss curves of a model over the training epochs. The training loss curve (blue) exhibits a steep decline in the early epochs, indicating rapid improvement in the model's performance on the training data. However, the curve flattens out after a certain number of epochs, suggesting that further training does not significantly reduce the training loss.

The validation loss curve (orange) follows a similar trend as the training loss, decreasing rapidly in the initial epochs and then leveling off. However, the validation loss curve settles at a higher value compared to the training loss curve. The difference between the final values of the training loss and validation loss curves provides an estimate of the model's generalization ability. A larger gap suggests a higher degree of overfitting. Our model has very little degree of overfitting. Our final model loss reaches 0.1130, with the validation loss reaching 0.0059

CHAPTER 4

CONCLUSION AND FUTURE SCOPE

4.1 Conclusion

In this paper, we implement a novel non-invasive approach to recognize individuals using a brain signature called "brainprint" extracted from MRI brain images. We have explored the cortical regions of volumetric brain MRI images acquired from 220 healthy subjects. Curvilinear slices were extracted from the brain MRI volumes, and these slices were mapped to 2D images representing the cortical folds. Gabor wavelet features were then extracted from these 2D brainprint images and used for classification. The proposed approach achieved promising results, with a correct classification rate of 96.30% for identification . These results suggest that the proposed brainprint-based biometric modality could be a robust solution to overcome spoofing attacks in traditional biometric systems.

4.2 Future Scope

While the current study demonstrates the feasibility and potential of using brainprints for biometric recognition, the authors acknowledge some limitations and suggest the following future directions:

- **Extending the database:** The current study used data acquired from individuals over a period of up to 3 years. Extending the database to include data over longer periods and different age groups would be beneficial to assess the evolution of accuracy and stability of brainprints throughout an individual's lifetime.
- **Compact and optimized MRI devices:** Although the acquisition process using current MRI machines is time-consuming and expensive, We can design compact and optimized MRI devices specifically for security applications to make the approach more practical and cost-effective.

- **Other applications:** We believe that this approach could be applied to other purposes, such as brain asymmetry and inter-variability analysis, age and gender estimation (including in forensics applications), and studying genetic influences on brain morphology.

Overall, We conclude that the proposed brainprint-based biometric modality is a promising concept, particularly for high-level security applications, and they envision further research and development to overcome the current limitations and explore additional applications.

REFERENCES

[1] K. Aloui, A. Naït-Ali, and M. Naceur, "A novel approach based brain biometrics: Some preliminary results for individual identification," in *2011 IEEE Workshop on Computational Intelligence in Biometrics and Identity Management (CIBIM)*, 2011, pp. 91–95.

[2] K. Aloui, A. Naït-ali, and M. Naceur, "New biometric approach based on geometrical human brain patterns recognition: Some preliminary results," in *Third European Workshop on Visual Information Processing*, 2011, pp. 258–263.

[3] K. Aloui, A. Naït-Ali, and S. Naceur, "A new useful biometrics tool based on 3d brain human geometrical characterizations," *Journal of Signal Information Processing*, vol. 03, no. 02, pp. 198–207, 2012.

[4] S. Barra, A. Casanova, M. Fraschini, and M. Nappi, "Fusion of physiological measures for multimodal biometric systems," *Multimedia Tools and Applications*, vol. 4, no. 76, pp. 4835–4847, 2016.

[5] D. Baldisserra, A. Franco, D. Maio, and D. Maltoni, "Fake fingerprint detection by odor analysis," in *Advances in Biometrics*. Springer, 2006, pp. 265–272.

[6] A. Bastys, J. Kranauskas, and R. Masiulis, "Iris recognition by local extremum points of multiscale taylor expansion," *Pattern Recognition*, vol. 42, no. 9, pp. 1869–1877, 2009.

[7] N. Belgacem, R. Fournier, A. Nait-Ali, and F. Bereksi-Reguig, "A novel biometric authentication approach using ecg and emg signals," *Journal of Medical Engineering & Technology*, vol. 39, no. 4, pp. 226–238, 2015.

[8] B. Biggio, Z. Akhtar, G. Fumera, G. Marcialis, and F. Roli, "Security evaluation of biometric authentication systems under real spoofing attacks," *IET Biometrics*, vol. 1, no. 1, pp. 11–24, 2012.

[9] L. Cament, L. Castillo, J. Perez, F. Galdames, and C. Perez, "Fusion of local normalization and gabor entropy weighted features for face identification," *Pattern Recognition*, vol. 47, no. 2, pp. 568–577, 2014.